# ICESat-2 Data Application for DEM Bias Compensation Based on Point-to-Surface Matching

Hyoseong Lee and Michael Hahn

***Abstract*— Creating high-quality digital elevation models (DEMs) from high-resolution satellite images requires an accurate sensor model. Rational polynomial coefficients (RPCs) have been widely employed instead of rigorous sensor models. However, the generated DEMs can be distorted because of the inherent RPC biases. Conventionally, the bias is compensated by incorporating ground control points (GCPs) into the standard processing workflow, which requires additional effort to measure the ground and image coordinates of the GCPs. Furthermore, in an inaccessible area, such as polar regions, it is difficult to perform field surveying of ground coordinates. In this study we investigate whether and how the data recorded by NASA's Ice, Cloud, and Land Elevation Satellite-2 (ICESat-2) mission can be used as GCPs without requiring an operator to measure the image coordinates. The first step is generating DEMs by image matching from high-resolution satellite images with the given RPCs. A point-to-surface matching method that matches the ICESat-2 data to the DEM surface was developed to correct the DEM and improve its precision. For the experimental investigations, we use KOMPSAT-3 imagery and ICESat-2 ATL08 data for a Korea test site and KOMPSAT-3A imagery along with ICESat-2 ATL06 and ATL08 data for a test site at the Thwaites Glacier in Antarctica. For the Korea test site, we additionally perform a land cover classification to select ATL08 segments that are uniquely assignable to the terrain surface. After point-to-surface matching, the DEMs are corrected in both test areas. The accuracy analyses show that the proposed method improves the accuracy (root mean square error) of the corrected DEM from 10 m to 2 m for the Korea test site and from 14 m to 1 m for the Antarctic test site. Furthermore, we placed particular emphasis on the terrain slope. To investigate the impact of terrain slope on the bias compensation process, we separate the ATL08 data of the Korea test site into groups of different terrain slope. It turns out that the deviation of the ATL08 data is lowest at about 1 m when the DEM slope is within 10°. Beyond a 30° slope, the RMSE increases by a factor of 7 compared to the 0-10° range.**

***Index Terms*—Point-to-surface matching, ICESat-2 data, digital elevation model (DEM), rational polynomial coefficient (RPC), land cover classified image**

This work was supported in part by the Ministry of Education of the Republic of Korean and the National Research Foundation of Korea (NRF-2018R1D1A1B06049484). Additionally, we would like to thank the Korea Aerospace Research Institute for their provision of the image data. Hyoseong Lee (*corresponding author*) is with the Department of Civil Engineering, Sunchon National University, Suncheon 57922, South Korea (email: hslee@scnu.ac.kr), and Michael Hahn is with the Department of Geomatics, Computer Science and Mathematics, Stuttgart University of Applied Sciences, Stuttgart, 70174, Germany (email: Michael.Hahn@hft-stuttgart.de).

## I. Introduction

The quality of the digital elevation models (DEMs) generated using 3D stereographic high-resolution satellite imagery depends on the accuracy of the sensor orientation or the rational polynomial coefficients (RPCs). The RPCs are a set of parameters that are used to relate object space coordinates to image space coordinates through a rational function [1]. RPCs are extensively employed owing to their simplicity and convenience in the photogrammetric process compared with rigorous sensor orientation. Numerous studies in the past two decades have shown that meter-level accuracy can be achieved by the RPC geopositioning of high-resolution imaging satellites [2], [3].

This strategy requires one or more ground control points (GCPs). These are points in the terrain with known coordinates in an appropriate terrain coordinate system, and which are clearly identifiable in satellite or aerial images. Typically, GCPs are established on-site through Global Positioning System (GPS) measurements. The photogrammetric process involves determining the image coordinates of these GCPs, which can then be used to correct the bias of the RPCs associated with the satellite images.

Early studies, such as that of Ebner et al. [4], reported that, under ideal conditions of well-defined and recognizable ground points and precise image measurements, a point determination of 0.3 pixels is possible. In practice, accuracies between 0.5 and 2 pixels are often observed. Providing GCPs can be hindered or time-consuming in certain areas when fieldwork such as GPS surveying is required. This is particularly true in the Arctic and Antarctic polar regions, where it is difficult to collect GCPs. Accurate and up-to-date DEMs are required in polar regions to estimate changes in sea ice thickness, quantify melting ice sheets, and monitor sea level changes [5].

To compensate for the DEM generated from stereo satellite images, approaches that do not rely on conventional GCPs have been pursued based on combined point determination using a reference DEM [6], [7]. This approach is known as the least height difference (LHD) algorithm, in which the transformation parameters between the DEM points and reference surface points are iteratively estimated by minimizing the sum of the squared height differences on the same horizontal location. Kim and Jeong [8] investigated the suitability of the LHD algorithm for accurate mapping of satellite images. They found that the three-dimensional similarity transformation becomes

apparent when errors occur solely in the form of time-invariant position and attitude biases within the coordinate frame of push-broom satellite images. Chen et al. [9] employed a Shuttle Radar Topography Mission (SRTM) DEM for the RPC correction of images obtained from the TianHui-1 satellite based on the LHD algorithm. They improved the planimetric and vertical accuracies from tens of meters to within 10 m, which is suitable for topographic mapping at a scale of 1:50,000. Cao et al. [10] evaluated the dependability of three pre-existing global DEMs to enhance the accuracy of a sensor model of numerous images from the ZY-3 satellite through bundle adjustment using the LHD algorithm. The experimental result indicated that the horizontal and vertical root mean square errors (RMSEs) of the images were reduced from 17.3 m and 2.6 m to 2.5 m and 1.5 m, respectively. They concluded that geopositional accuracy depends on the quality and accuracy of the global DEM. However, it is possible that the LHD transformation can become ill-posed in situations with large slopes [11]. In particular, the planimetric parameters in translations depend exclusively on the effect of the slope [12].

Other researchers have attempted to improve the DEM accuracy using location data obtained from NASA's Ice, Cloud, and Land Elevation Satellite-2 (ICESat-2) mission. Magruder et al. [13] presented an automated method for correcting the elevation of an SRTM DEM using ICESat-2 data combined with Landsat 8 imagery. A reduction in the biases of the SRTM elevations of more than 50% was achieved after applying the method. Zhang et al. [14] proposed an RPC joint block adjustment method using selected ICESat-2 ATL03 data to improve the geopositioning accuracy of triple stereo images of the ZY3-02 satellite. The accuracy of the experimental results was increased by more than 56%. This technique requires the deployment of suitable ATL03 points in mountainous areas. Ye et al. [15] proposed an integration strategy based on terrain similarity (BOTS) between ICESat-2 ATL03 data and a digital surface model (DSM) to improve DSM elevation accuracy from optical satellite images. Using the proposed method, the DSM elevation accuracy increased by 73–92%. To compute terrain features, the BOTS algorithm requires a sufficient number of points; therefore, the authors recommended using ATL03 data with a higher point density rather than the sparser ATL08 data.

Wang et al. [16] experimentally determined that the slope of the terrain is the most influential source of error affecting the elevation accuracy of ATL03 data. They found that “elevation errors increase rapidly with increasing slope, especially when the slope is greater than 20° [16].” Tian and Shan [17] found “that for terrain modelling under forest, a significant majority of ATL08 product may not be useful” and among the useful ones they may still have outlier elements. Outliers occur where the terrain is rough, has dense vegetation or where buildings exist. They also reported that the accuracy of the ATL08 terrain height significantly decreases in areas with large slopes or large canopy coverage [17]. How the slope at the location of the ATL08 data affects our processing results is analyzed for the first test site in Section 4. In the upcoming section (Data and Methods), we delve into the background of the employed ICESat-2 data and elaborate on the selected investigative methodology. Subsequently, Section 3 provides a concise overview of the point-to-surface matching method. Experimental investigations on the correction of DEMs generated from KOMPSAT-3 and KOMPSAT-3A stereo images are then described and discussed in Section 4. Finally, Section 5 summarizes the results obtained using ICESat-2 data to improve the accuracy of the DEMs.

## II. Data and Methods

ICESat-2 was launched in September 2018, with scientific objectives that focus on measuring the changes in the land and sea ice in the cryosphere. ICESat-2 analyzes melting ice sheets and estimates the thickness of sea ice to monitor sea level changes in Greenland and Antarctica. Although the primary mission of ICESat-2 is to monitor changes in the cryosphere, it also collects data on terrestrial surfaces worldwide and measures the locations of topography, forest cover, and oceans [18].

The sole instrument onboard ICESat-2 is the Advanced Topographic Laser Altimeter System (ATLAS). The ATLAS can take measurements every 0.7 m along the satellite’s ground path, and the footprint of each pulse has a diameter of approximately 17 m on the Earth’s surface. The diffractive optical element in ATLAS splits the laser beam into three pairs that are spaced approximately 3 km at the surface. Each beam pair consists of strong- and weak-energy beams, and the energy of the strong beam is approximately four times higher than that of the weak beam. [19].

The ICESat-2 mission provides various types of surface geophysical products ranging from ATL01 to ATL21. ATL03 is a Level-2 product containing the time, latitude, longitude, and height above the World Geodetic System 1984 (WGS 84) ellipsoid for each photon. The mission provides comprehensive photon information for Level-3A data products, such as land ice elevation (ATL06), sea ice elevation (ATL07), and land and vegetation elevation (ATL08). The ATL06 product offers ground surface elevation in polar regions, whereas ATL08 provides both the terrain and tree canopy elevations in non-polar regions and ground-surface elevation in polar regions. The ATL06 and ATL08 surface elevation data are derived from aggregated estimates that are extracted from segments of the ATL03 point data [20].

ICESat-2 products, including ATL06 and ATL08, can be sourced from the National Snow and Ice Data Center (NSIDC) [18]-[20]. In addition, the ICESat-2 data is readily accessible and can be downloaded from NASA’s OpenAltimetry (https://openaltimetry.org/data/icesat2/). The ICESat-2 mission has horizontal and vertical accuracies of greater than 6.5 m and 10 cm, respectively [15]. Brunt et al. [21] reported that the accuracy of the ATL06 elevation measurement over the Antarctic ice sheet was approximately ±5 cm, and the study by Neuenschwander and Magruder [22] of the ATL08 elevations for the terrain and canopy over a test area on land yielded RMSE values of ±0.85 m and ±3.2 m, respectively.

For this study, we designed a workflow in which we use ICESat-2 data as GCPs to improve the accuracy of DEMs from

high-resolution satellite stereo pairs. The processing sequence is as follows: The DEM from high-resolution satellite images and ICESat-2 ATL08 and ATL06 data are fed into the point-to-surface matching algorithm, developed by the authors in previous works [23], [24]. The matching process is fully automated and does not require operator interaction. Matching between the ATL08/ATL06 data and the DEM provides the estimated parameters of the geometric transformation between the coordinates of the segments and the DEM. The DEM is then corrected using the transformation parameters.

Two test sites have been selected for the experiments: one on the Korean Peninsula and the other at the Thwaites Glacier in Antarctica. The first experiment involves the use of a pair of stereo KOMPSAT-3 images from the Korean Peninsula and ICESat-2 ATL08 data. A land cover map generated by image classification ensures that only the ICESat-2 ATL08 data that are uniquely assignable to the terrain surface are used as GCPs. The accuracy of the corrected DEM is validated using secured ground-truth check points. In the second experiment, an Antarctic DEM was generated using a KOMPSAT-3A stereo image pair. ICESat-2 ATL06 and ATL08 data are used as the GCPs for point-to-surface matching. Finally, the two corrected DEMs are compared accordingly. However, check points, such as recorded GPS points, were not available for this region.

## III. Point-to-Surface Matching Model

The matching approach aims to determine the transformation parameters between the ICESat-2 data locations used as GCPs and the surface of a DEM, which consists of 3D translation and 3D rotation, as well as a scale parameter such that the sum of the squared distances between the points and the surface is minimized (Fig. 1(a)).

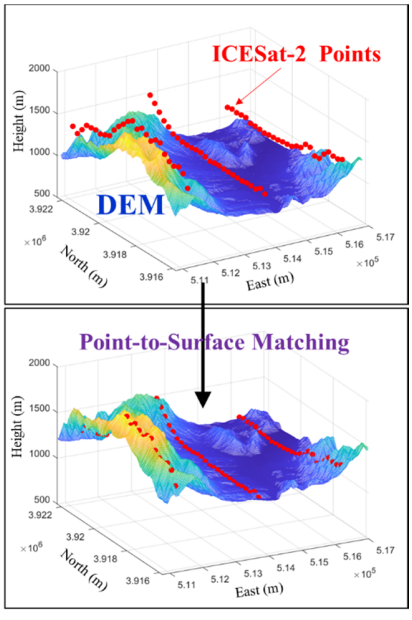


(a)

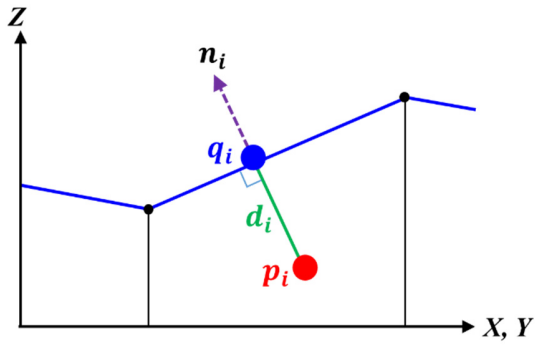


(b)

Fig. 1. Illustration of (a) point-to-surface matching between the ICESat-2 data and the DEM surface based on the WGS 84 UTM coordinate system, and (b) distance measurement between the GCPs ($p_i$) and surface Z (X, Y) of the DEM [23], [24].

For the point-to-surface matching algorithm, we employed the shortest distance $d_i$ from point $\boldsymbol{p}_i$ to the surface at point $\boldsymbol{q}_i$ in the DEM, as shown in Fig. 1(b) [23] and [24]. This can be formulated as an optimization to determine the corresponding point $\boldsymbol{q}_i$ by determining the shortest distance $d_i$ from point $\boldsymbol{p}_i$ to the surface. If a surface patch is described by a plane, as sketched in Fig. 1(b), the process is straightforward, because any point on the plane can be applied to compute the distance $d_i$ of point $\boldsymbol{p}_i$ from the plane based on

$$d_i = \frac{\boldsymbol{n}_i^T}{|\boldsymbol{n}_i|}(\boldsymbol{p}_i - \boldsymbol{q}_i) \tag{1}$$

where $i$ indicates the $i^{\text{th}}$ point, $\boldsymbol{n}_i$ is the normal vector, $\boldsymbol{p}_i$ is the ICESat-2 point location used as the GCP, and $\boldsymbol{q}_i$ is the location of the corresponding point on the surface. For nonplanar surface patches such as bilinear surfaces, the optimization can be solved iteratively by approximating the tangential planes for which the best matching point $\boldsymbol{q}_i$ can be tracked.

A 3D similarity transformation model is used to express the geometric relationship between the GCP and the corresponding point on the surface as follows:

$$\boldsymbol{p}_i^* = \boldsymbol{s}\boldsymbol{R}\,\boldsymbol{p}_i + \boldsymbol{t} \tag{2}$$

where $\boldsymbol{p}_i^*$ is the location of the transformed $\boldsymbol{p}_i = [X\ Y\ Z]_i^T$, $\boldsymbol{s}$ is a scale factor, $\boldsymbol{R} = R(\omega, \varphi, \kappa)$ is the 3D rotation matrix, and $\boldsymbol{t} = [t_x\ t_y\ t_z]^T$ is a 3D translation vector.

The final location $\boldsymbol{q}_i$ is estimated by least-squares minimization, $\boldsymbol{e}$ represents the sum of the squared distances between $\boldsymbol{p}_i^*$ and the search surface elements:

$$e = \sum_{i=1}^{N} d_i^2 \tag{3}$$

The least-squares method for point-to-surface matching is derived directly by considering the GCP $\boldsymbol{p}_i$ outside the surface. To perform the least-squares estimation, assuming that the

DEM is modeled implicitly by $F(X,Y,Z)=0$, $F$ should be linearized using the Taylor series expansion (omitting index $i$ for simplicity):

$$\begin{aligned} F(X,Y,Z) = {} & F(X^0,Y^0,Z^0) \\ & + \frac{\partial F(X^0,Y^0,Z^0)}{\partial X} dX \\ & + \frac{\partial F(X^0,Y^0,Z^0)}{\partial Y} dY \\ & + \frac{\partial F(X^0,Y^0,Z^0)}{\partial Z} dZ \end{aligned} \tag{4}$$

with

$$\begin{aligned} \frac{\partial F(X^0,Y^0,Z^0)}{\partial X} &= n_x\,, \\ \frac{\partial F(X^0,Y^0,Z^0)}{\partial Y} &= n_y\,, \\ \frac{\partial F(X^0,Y^0,Z^0)}{\partial Z} &= n_z \end{aligned} \tag{5}$$

$$dX = \frac{\partial X}{\partial k_j} dk_j,\quad dY = \frac{\partial Y}{\partial k_j} dk_j,\quad dZ = \frac{\partial Z}{\partial k_j} dk_j \tag{6}$$

where $dk_j \in \{\, dt_x, dt_y, dt_z,\ d\omega, d\varphi, d\kappa,\ ds \,\}$ is the $j^{\text{th}}$ transformation parameter in (2), $n_x, n_y$, and $n_z$ are the X-Y-Z components of $n$.

In the least-squares approach, suitable approximate values are required for the geometric transformation parameters. When matching the GCPs to a DEM, it can be assumed that a scale factor $s=1$, rotation matrix $\boldsymbol{R}=\boldsymbol{E}$, and translation vector $\boldsymbol{t}=\boldsymbol{0}$ are suitable starting values for $F(X^0,Y^0,Z^0)$ of (4).

$$F(X^0,Y^0,Z^0) = d^o - \frac{n_o^T}{|n_o|}(p^o - q^o) \tag{7}$$

where index ( $^o$ ) is the approximation, and $p^o$ is iteratively transformed to a new state using the updated $dk_j$ in (1) and (2). In the present implementation, point $q^o$ is determined by bilinear interpolation on the DEM surface using the $X,Y$ coordinates of $p^o$.

The linearized model of (4) leads to the following matrix notation:

$$\boldsymbol{v} = A\boldsymbol{x} - l \tag{8}$$

where $\boldsymbol{A}$ is the design matrix, $\boldsymbol{x} = (d\omega, d\varphi, d\kappa, dt_x, dt_y, dt_z)^{\boldsymbol{T}}$ is the vector with the geometric transformation parameters, and $\boldsymbol{l} = F(X^0,Y^0,Z^0)$ represents the observation vector.

Minimizing the sum of the weighted squared distance $\boldsymbol{e}$ of (3) results in the standard least-squares estimates of the parameters:

$$\hat{\boldsymbol{x}} = (\boldsymbol{A^T P A})^{-1}\boldsymbol{A^T P l} \tag{9}$$

The weight $\boldsymbol{P}$ should be determined appropriately. The distance $(d_i)$ of any point $(i)$ must not be significantly different from those of the other points. Therefore, a simple weighting scheme was adopted:

$$P = \begin{cases} 1 & \text{if } |d_i - mean(d_i)| < 2.0\sigma \\ 0 & \text{else} \end{cases} \tag{10}$$

To eliminate the outliers (points representing gross errors), only the points where $d_i$ is within $2.0\sigma$ ($\sigma$ is the standard deviation of $d_i$) can participate in the matching. The transformation parameters were determined when the estimated value of $\hat{\boldsymbol{x}}$ approached zero. This adjustment is performed iteratively. In each iteration, the unknowns are updated using the results of (8), such as ${t_x}^1 = {t_x}^0 + dt_x$, ..... The convergence behavior of the proposed method relies on the qualities of both the initial approximations and data content. For further details on the matching iteration process, please refer to [23].

## IV. Experimental Investigations and Results

For our experimental investigations we utilized a KOMPSAT-3 image pair and ATL08 data for the land test site in Korea, and a KOMPSAT-3A image pair along with ATL06 and ATL08 data for the test site in Antarctica. Vendor-provided RPCs were readily available for both of these test sites. The workflow for generating and correcting the DEMs in both locations is illustrated in Fig. 2. The photogrammetric process of DEM generation uses the image pairs and utilizes the provided RPCs. ICESat-2 data were employed in point-to-surface matching to determine the bias transformation parameters, which ultimately led to the correction of the DEM.

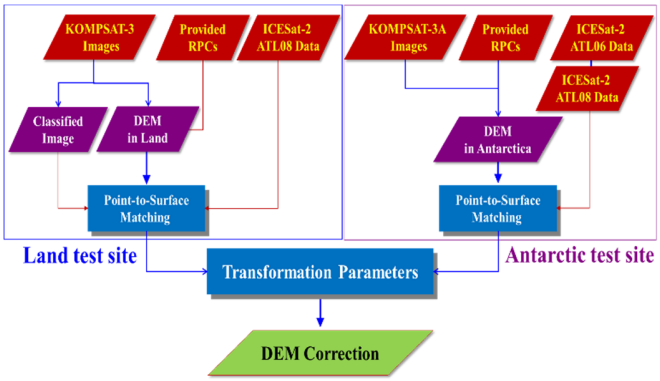


Fig. 2. Workflow of using ICESat-2 data for correcting DEMs.

A particular feature of the processing at the land test site is the incorporation of image classification, which is used to ensure that only bare ground locations are considered in the point-to-surface matching. From the ATL08 data, the terrain height points with an uncertainty of 1.0 m or less are selected. The uncertainty values are provided by the OpenAltimetry website. Canopy heights of the ATL08 data are not considered. Early experiments with ICESat and SRTM DEMs have already pointed to reduced DEM accuracies in forest areas [25], [26]. A larger time difference between the recording of ICESat data and KOMPSAT images would exacerbate issues of tree cover in vegetated areas.

For processing at the Antarctic test site, ATL06 and ATL08 data were used. ATL06 provides quality values for the land ice height [20], and data with a quality rating of 0 (zero), indicating

good reliability, were selected. As with the land test site, height data with an uncertainty of less than 1.0 meter were extracted from the ATL08 data.

Table I lists the specifications for the two panchromatic satellite image pairs.

TABLE I. SPECIFICATIONS OF THE IMAGES USED.

| | KOMPSAT-3 (Test site # 1) | | KOMPSAT-3A (Test site # 2) | |
|---|---|---|---|---|
| ID | K3-1 | K3-2 | K3A-1 | K3A-2 |
| Acquisition date/time | 02-25-2013 /04:33 | 02-25-2013 /04:34 | 03-19-2016 /23:16 | 03-19-2016 /23:17 |
| Image size (km) | 16.84 × 16.53 | 16.84 × 16.63 | 12.03 × 9.17 | 16.84 × 9.07 |
| Spatial resolution (m) | 0.7 × 0.8 | 0.7 × 0.8 | 0.5 × 0.6 | 0.7 × 0.6 |
| Roll angle (°) | 6.6 | 5.0 | 23.8 | 23.9 |
| Pitch angle (°) | 13.8 | -14.2 | -27.2 | 27.5 |
| Yaw angle (°) | -3.0 | -3.4 | 13.4 | -12.1 |

### *A. First test site*

#### *1) Data Preparation*

The first land-surface test site is Suncheon City, situated in the south of the Korean Peninsula (Fig. 3). The KOMPSAT-3 images cover an area of approximately 17 × 16 km in Suncheon City, whose mountainous regions are densely forested. As indicated in Table I, the ground resolutions of the two images are 0.7 m and 0.8 m, respectively. The roll and yaw angles of both images are pointing in similar directions, while the signs of the pitch angles differ. The test site offers diverse possibilities to assess the suitability of the ICESat-2 data.

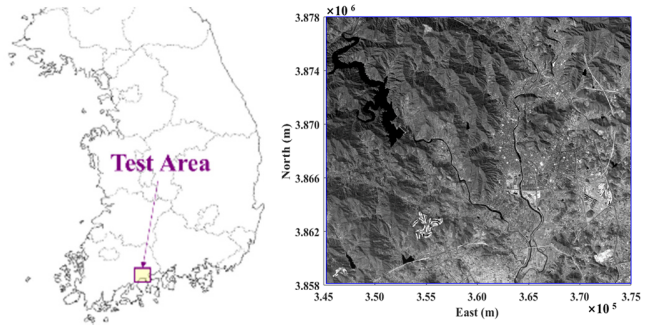


(a) (b)

Fig. 3. (a) Map of the South Korean peninsula and test area (purple box) in Suncheon City. (b) Sample image of KOMPSAT-3 stereo pair for Suncheon based on the WGS 84 UTM coordinate system.

The ATL08 elevation data recorded in November 2019 and April 2020 were downloaded from the OpenAltimetry website and used in this study. There is an approximate seven-year time gap between capturing of the KOMPSAT-3 images and ICESat-2 data. For the point-to-surface matching investigations (Fig. 4(a)), we had access to 702 ATL08 points for 2019.

In this area, 21 national control points (NCPs) and 31 public control points (PCPs) were available, which can be used to perform independent estimates of the DEM transformation parameters and alternatively as ground truth to assess the accuracy of the corrected DEM. Most NCPs and PCPs were established throughout South Korea by the Korean National Geographic Information Institute in 2012 and 2017, respectively. Data were acquired through geodetic measurements using a Global Navigation Satellite System (GNSS) and geodetic network processing. Since NCPs and PCPs were clearly identifiable in the KOMPSAT-3 image pair, they were suitable as independent control points (ICPs) to assess the matching accuracy. Fig. 4(a) depicts the ATL08 points and ICPs within the project area. Furthermore, we used an additional 663 ATL08 points collected in 2020 (Fig. 4(a)) to analyze the elevation accuracy according to various levels of the terrain slope.

A DEM with 2 m grid spacing was generated from the KOMPSAT-3 image pair and the RPCs using SimActive's Correlator3D software at the test site (Fig. 4(b)). The generation was conducted using WGS 84 UTM coordinates as the foundation, allowing for an immediate comparison with the coordinates of the ICESAT-2 data and the ICPs.

The generated DEM does not represent the ground in forest regions, but an approximation the canopy surface. In principle the ATL08 heights for the canopy and not for the terrain would therefore be an option for the matching process at those locations. Due to the aforementioned problems in forested areas, we refrain from this option and focus on ground height points.

#### *2) DEM bias compensation with categorized ATL08 data*

As a strategy for a reliable selection of segments representing ground elevation from the ATL08 data, we classify the multispectral KOMPSAT-3 image. Fig. 4(c) displays the classification image created with the ERDAS software. The land cover classes forest, water, urban and ground were defined for the supervised classification with the maximum likelihood method.

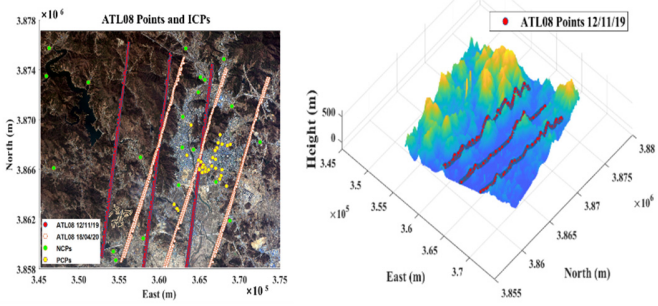


(a) (b)

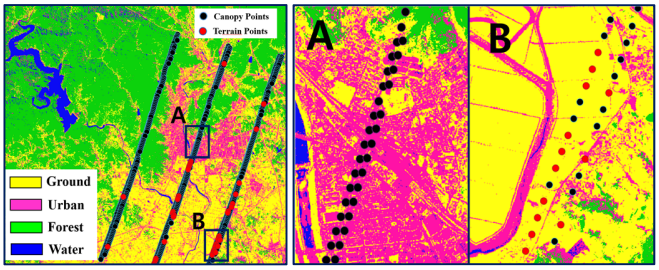


Fig. 4. (a) Plot of ATL08 data recorded in 2019 (red circles), in 2020 (magenta circles), NCPs (green circles) and PCPs (yellow circles) in front of the multispectral image. (b) DEM and overlay of the ATL08 points from 2019 (red dots). (c) Land cover classified image and ATL08 2019 segments overlay of the canopy (black dots) and terrain height points (red dots). (d) Canopy and terrain points in zoomed windows A and B overlaid to the classification image.

By overlaying the ATL08 data, in which tree and terrain heights are present at the same location, onto the land cover image (cf. Fig. 4(d), A and B), we notice that urban areas, agricultural areas without crops, and bare land indicate erroneous ATL08 tree canopy height data. In contrast, the ATL08 terrain elevation data (for which no tree canopy height is given) located in the agricultural areas or bare land are shown correctly. However, the number of those segments is quite low as there are only 42 out of 702 points. To increase this number, it is advisable to use the land cover images to obtain a larger number of points from the ATL08 data that correspond to the ground.

Fig. 5 shows the ATL08 data categorized into three classes without taking uncertainty into account: 237 forest segments, 376 ground segments, and 89 urban segments. Agricultural and bare land are grouped into ground areas, which means that grassland and other ground areas fall into one category. Fig. 6 visualizes the categorized segments, allowing a visual assessment of the classification accuracy of the segments.

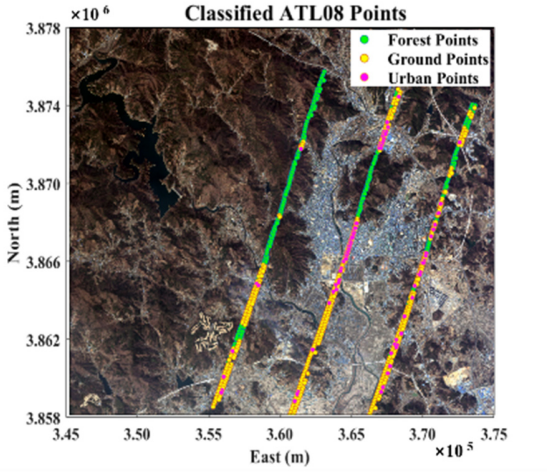


Fig. 5. Distribution of the three categories of ATL08 segments overlaid on the multispectral image.

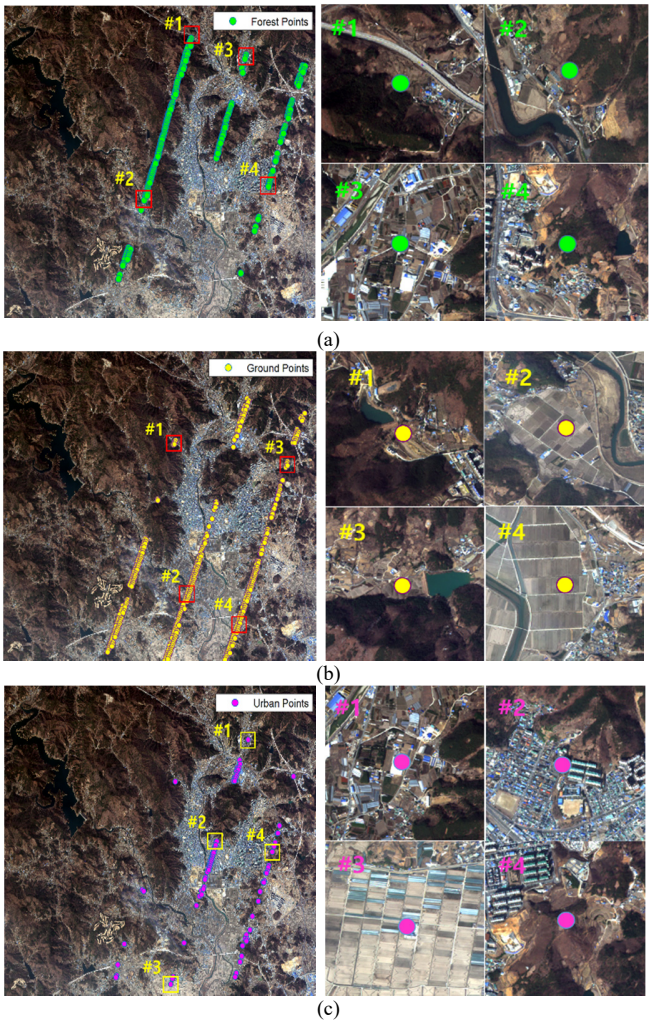


Fig. 6. Categorized ATL08 segments with (a) forest points, (b) ground points, (c) urban points and some zoom-in windows used for visual inspection.

For the visual inspection of the ATL08 data categorized by land cover classification, we aimed to use a sample of approximately 100 data points per category. In fact, we inspected all 89 urban points, 121 forest points, and 125 ground points within the zoom window. Two examples of misclassification are shown in window #3 in Fig. 6(a) where a forest segment was categorized as urban; and in window #4 in Fig. 6(c) where an urban segment was categorized as forest.

The visual validation resulted in a classification accuracy of 95% for forest, 82% for soil, and 81% for urban areas (Table II). Restricted to the 115 ground points with an uncertainty of less than 1 m that were used for the point-to-surface matching, the classification accuracy is 96 %.

TABLE II. CLASSIFICATION ACCURACY OF THE CATEGORIZED POINTS

| Class | Forest | Ground | | Urban |
|---|---|---|---|---|
| Uncertainty (m) | - | - | < 1.0 m | - |
| Sampled points | 121 | 125 | 115 | 89 |
| Wrongly categorized | 6 | 22 | 5 | 15 |
| Accuracy (%) | 95 | 82 | 96 | 81 |

The determination and evaluation of the deviations of the ground elevation heights in the ATL08 data locations are considered in the following for points that had an uncertainty of less than 1 m. These were 110 points of the category ground, 41 points of the category urban and 2 points of the category forest. Since the number of forest points is very low, the uncertainty level for the forest category was raised to 10 m, resulting in 19 points for the forest category. In addition, a fourth category was formed, labelled 'all points' in Table III which aggregates points from the three categories that meet the condition of having an uncertainty of less than 1 m.

Fig. 7 displays the points of the four categories. It is noticeable that 102 of the selected ground points are situated in the low-lying regions of the test area (cf. Fig. 7(c)), where minimal topographical changes have taken place in the past decade. The seven-year temporal gap between DEM and ICESat-2 data capture is expected to have a negligible impact in these locations. This may not be the case in urban areas, where redevelopment has occurred in recent years.

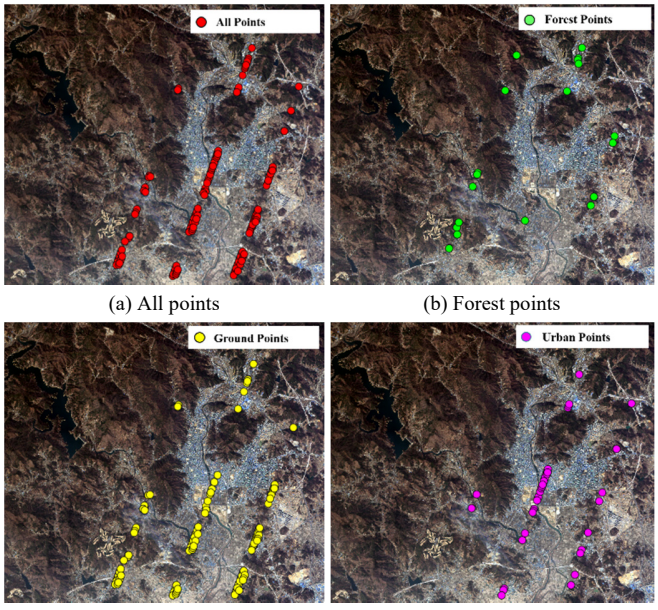


(a) All points (b) Forest points

(c) Ground points (d) Urban points

Fig. 7. ATL08 data subdivided into the following categories: (a) All points (uncertainty < 1 m), (b) forest points (uncertainty < 10 m), (c) ground points (uncertainty < 1 m), and (d) urban points (uncertainty < 1 m).

Table III summarizes the results of point-to-surface matching and DEM bias compensation separately for the four categories: all points, forest, ground and urban. The RMSE and the maximum distance between the point locations and the DEM surface indicate the influence of the ATL08 data of the respective category. Overall, the distance errors in each of the four categories have been significantly reduced by the bias compensation, for the RMSE from 16-23 m to about 0.5-5 m and for the maximum distance error from 23-30 m to about 1.4-17 m (Table III). The maximum distance errors of the 'all points' category and the forest data category are with around +10 m drastically bigger as those of the data of the ground and urban category. As a result, these segment classes are less suitable for DEM bias compensation.

Table III highlights the ATL08 segments of category ground with a notable RMSE value of 21.2 m before the DEM correction, which significantly reduces to 0.5 m after the correction. Furthermore, the maximum deviation after the correction is quite low, at just 1.4 m. These are strong indications that ATL08 segments located in open terrain are particularly suitable for bias compensation of the DEM.

TABLE III. DISTANCE ERRORS BETWEEN THE ATL08 AND SURFACE POINTS OF THE DEM BEFORE AND AFTER MATCHING.

| Category | All points (uncert. < 1 m) | | Forest | | Ground | | Urban | |
|---|---|---|---|---|---|---|---|---|
| Matching | Before | After | Before | After | Before | After | Before | After |
| RMSE (m) | 16.8 | 1.7 | 19.2 | 4.9 | 21.2 | 0.5 | 23.0 | 1.2 |
| Max (m) | 23.0 | 11.6 | 28.7 | 17.1 | 24.0 | 1.4 | 30.1 | 2.6 |

Fig. 8 visualizes the 2D and 3D displacements between the 102 points of the ground category, which turned out to be the most accurate among the ATL08 segments, and the surface points before and after the DEM correction. In these visualizations the displacements are magnified 100 times for clarity. Fig. 8(a) clearly shows the impact of translation and rotation within the 2D plane while Fig. 8(b) highlights the presence of errors in a few points even after the DEM correction. The situation for the displacements in 3D is similar, as can be seen in Figs. 8(c) and (d). In some of the points green vectors are visible and indicate displacement errors in the vertical direction.

From a quantitative point of view, the maximum absolute distance errors after DEM correction are 0.2 m in both the X and Y directions, while the maximum absolute error in the Z-direction is 1.4 m. It remains challenging to definitively determine whether this discrepancy represents an inherent height error in the ATL08 data or a height error within the generated DEM.

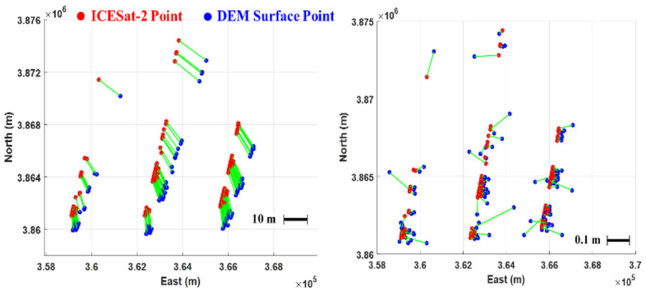


(a) (b)

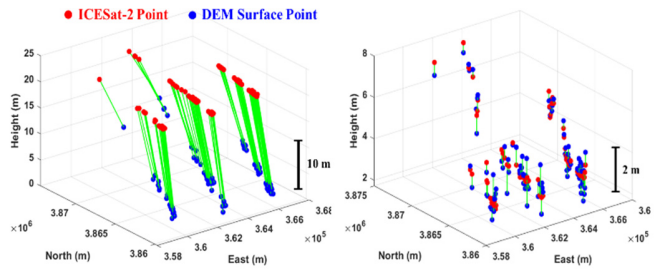


(c) (d)

Fig. 8. Visualization of the displacements between the ATL08 data (categorized as ground points) and surface points of the DEM before and after matching: 2D displacements (a) and (b) and 3D displacements (c) and (d).

For the independent accuracy assessment of the corrected DEM the ground truth ICPs were used. All these points were measured on the terrain surface and in open terrain. Therefore, the points could also be easily inspected in the KOMPSAT-3 image pair.

In Fig. 9, the distances of the 52 ICPs from the generated DEM (before DEM correction) are represented by black dots. The horizontal axis in this figure is labeled with point IDs (1 to 52). The process of matching the ATL08 data from the 4 categories led to the 4 corrected DEMs (for short we refer to them as the 'category DEMs'). These category DEMs are validated with the ICPs; the distances of the ICPs from their respective category DEM surface are visualised in color for better differentiation. The ground points (yellow) are consistently near-zero value, clearly indicating that the deviations of the ICPs from the DEM surface of the ground category are particularly small.

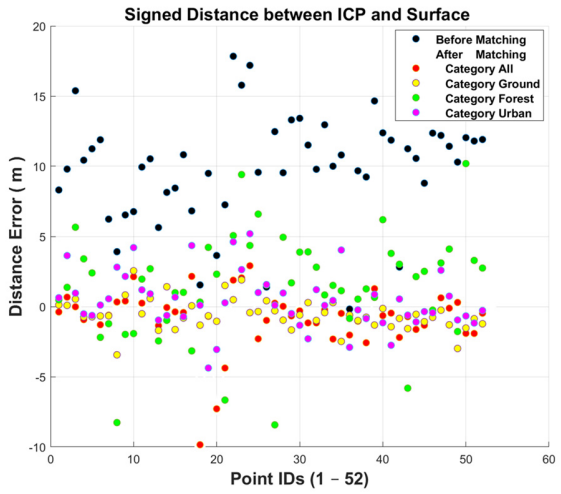


Fig. 9. Distance errors from the ICPs to the generated DEM (black) and to the category DEMs (colour).

Table IV quantifies the results shown in Fig. 9 for the four categories. It can be observed that, as previously noted in Table III, matching with the ATL08 data led to improvements of the corrected DEM across all four categories.

While the deviations from the DEM determined with the ICP check points were at 9.7 m (RMSE) and 16.4 m (max distance) before the DEM bias compensation, the use of ATL08 segments in the ground category resulted in a significant improvement, reducing the values to 1.2 m (RMSE) and 3.4 m (max distance). The distances were slightly greater for ATL08 points in urban areas and lead to similarly large distances in the remaining categories (see Table IV).

TABLE IV. DISTANCE ERRORS BETWEEN THE ICPS AND THE RECONSTRUCTED OR CORRECTED DEM SURFACE BEFORE AND AFTER MATCHING

| Distance error | Before matching | After matching | | | |
|---|---|---|---|---|---|
| | | All points | Forest | Ground | Urban |
| RMSE (m) | 9.7 | 2.2 | 3.9 | 1.2 | 2.0 |
| Max (m) | 16.4 | 9.8 | 10.2 | 3.4 | 5.2 |

These results prove that the ICESat-2 data, recorded on the terrain surface and validated by land cover classification, with an uncertainty < 1.0 m, are very well suited as GCPs for DEM bias compensation. We also determined that the 7-year gap between the DEM and ATL08 had little effect on our results.

*3) Investigations related to slope*

The studies conducted by Wang et al. [16] and Tian and Shan [17] suggest that terrain slope might influence the DEM bias compensation process. To investigate this, the 2019 ATL08 data were employed for point-to-surface matching and DEM-correction. This corrected DEM was taken as references for the height error analysis with the ATL08 data acquired in 2020. From this corrected DEM, a slope image was generated and used to assign the 2020 ATL08 data to slope ranges. The ATL08 dataset comprised 663 segments with 174 of them being categorized as 'ground' using the classification image. The uncertainty values of the ATL08 segments were not taken into account.

In Fig. 10(a) we can see the slope image and the 2020 ATL08 data categorized by the four slope ranges: 101 points between 0°-10°, 31 points between 10°-20°, 18 points between 20°-30°, and 24 points over 30°. In Fig. 10(b), signed distance errors between the ATL08 points and the corrected DEM are visualised. The ATL08 points, categorized into the four slope ranges, are highlighted using different colors in the figure. It is evident that the majority of errors in points with slopes between 0° and 10° scatter around zero, indicating minimal deviation. However, as slope increases the height errors rise, displaying a negative systematic deviation. Wang et al. [16], in their prior study, also noted a negative systematic deviation when they scrutinized the deviations between ATL03 data and an airborne lidar DEM.

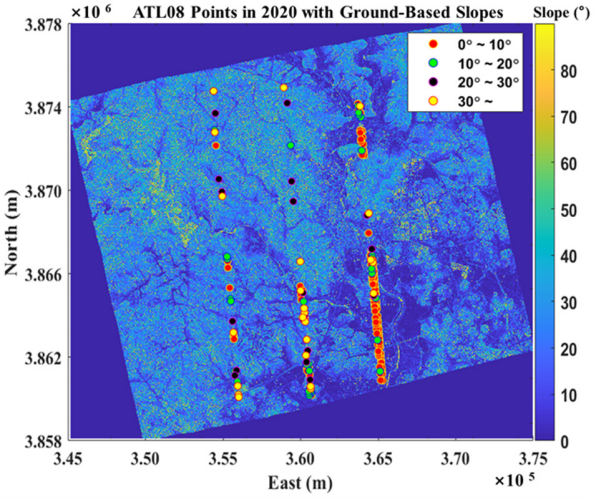


(a)

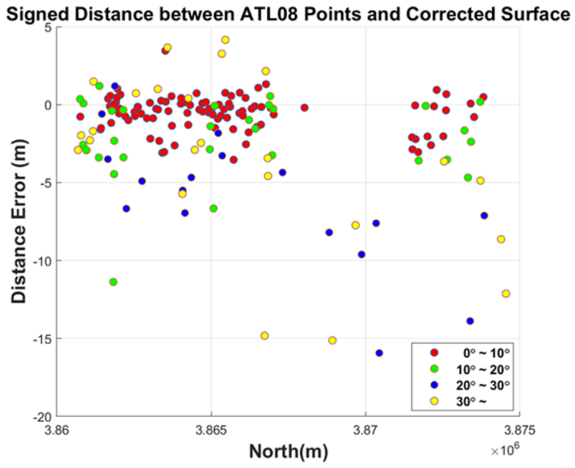


(b)

Fig. 10. (a) Point distribution ATL08 data categorized by slope range, and (b) signed distance errors between the ATL08 points and the corrected DEM surface.

The results presented in Fig. 10(b) are quantified numerically in Table V. As evident from this table, points with slopes below 10° have a maximum error of 3.5 m, and an RMSE of 1.2 m. The RMSE at points with slopes greater than 20° exceeds 7 m and distance errors (max) 15 m. Beyond a 30° slope, the RMSE increases by a factor of 7 compared to the 0-10° range.

This finding aligns with previous research, indicating that the error in ICESat-2 points increased rapidly beyond a slope of 20° compared to flat terrain and was nearly eight times higher in mountainous regions [16], [17].

Notably, the errors in points with slopes between 0° and 10° closely resemble those observed when ATL08 data were utilized for DEM correction, and ICPs were employed for evaluation (refer to Tables IV and V). These findings suggest that ICESat-2 data can effectively replace ICPs (collected during field surveys) for DEM bias compensation, which is especially advantageous in remote and inaccessible areas.

TABLE V. DISTANCE ERRORS BETWEEN THE ATL08 CHECK POINTS AND DEM SURFACE POINTS BASED ON THE SLOPES

| Distance error | Slope | | | |
|---|---|---|---|---|
| | 0° ~ 10° | 10° ~ 20° | 20° ~ 30° | 30° ~ |
| RMSE (m) | 1.2 | 3.3 | 7.4 | 8.6 |
| Max (m) | 3.5 | 11.4 | 15.9 | 20.0 |

## B. *Second test site*

The second test area is situated in proximity to the Thwaites Glacier in Antarctica (Fig. 11(a)). To achieve stereo capture of the test site, both images were taken with almost identical roll angles (approx. 24°) but with opposing pitch angles (approx. +27° for the first and -27° for the second image). Moreover, their respective yaw angles were about +13° and -12°. As shown in Table I, the image coverage spanned approximately 12 km x 9 km and 17 km × 9 km, influenced by the different ground resolution of the two images at 0.5 m x 0.6 m and 0.7 m x 0.6 m, respectively. The difference in resolution, particularly coupled with challenging surface texture (Fig. 11(b)) pose a challenge for image matching.

As with the first test site, a DEM with a grid spacing of 2 m was generated from the KOMPSAT-3A image pair and the RPCs for this test site using the Correlator3D software. Fig. 11 (c) shows the digital elevation model (DEM) created near the Thwaites Glacier, with an increased noise visible in the circled region of the DEM. In this region, numerous large and small crevasses are present. Image matching errors within the circled area result from shadows, occlusions, and discontinuities within and around these crevasses increase the noise in the DEM.

The ICESat-2 ATL06 and ATL08 data were captured concurrently in December 2018 and January, March, June, and August 2019. Within the DEM area, 2914 ATL06 points were used due to their very low uncertainty (< 10 cm) [21], and 512 ATL08 points were selected. Fig. 11(b) shows the ICESat-2 points in the sample image of KOMPSAT-3A stereo pair. The ICESat-2 points located within the yellow polygonal area, a very noisy region that accounts for 10 % of the total area (about 170 km$^2$) in the DEM (Fig. 11(c)), were excluded from consideration. However, the correction of the DEM with the parameters determined according to (9) is almost unaffected by the non-consideration of ICESat-2 data of this local region.

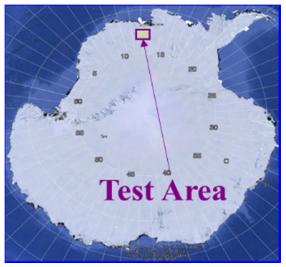


(a)

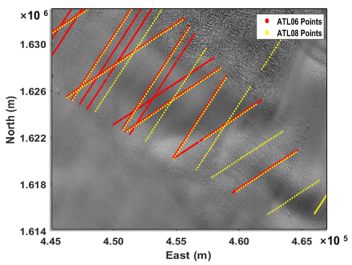


(b)

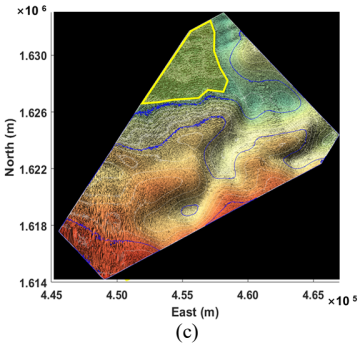


(c)

Fig. 11. (a) Location of the Antarctic test area near the Thwaites Glacier. (b) Distribution of the ICESat-2 ATL06 and ATL08 land-ice height points in the sample image (the coordinate system is UTM based on WGS 84) of the KOMPSAT-3A stereo pair of the test area. (c) Generated DEM.

After removing outliers using (10) and excluding noisy regions, a total of 1611 ATL06 and 320 ATL08 points were available for further analysis. The two data sets ATL06 and ATL08 were now used separately for point-to-surface matching and generation of two corrected DEMs.

Fig. 12 displays the DEMs before and after correction, along with the overlaid ATL08 points in the first column of the sub-images. The 3D distances between the ICESat-2 points and DEM surface points before and after the correction are depicted in the second column.

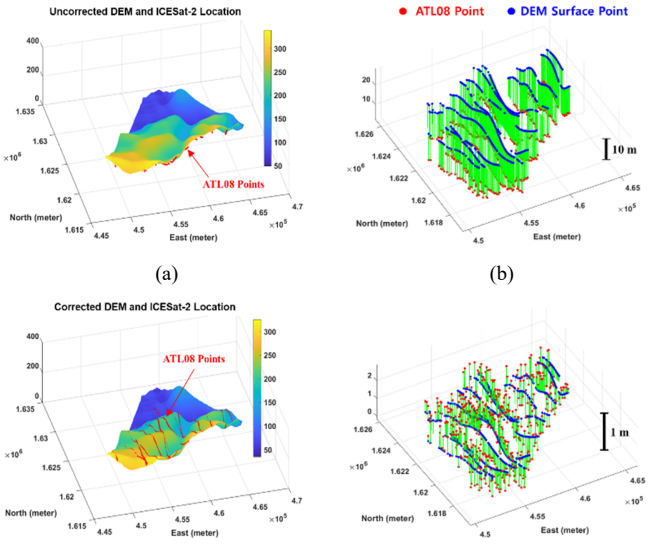


(a) (b)

(c) (d)

Fig. 12. ATL08 data (red dots) and DEM (a) before and (c) after matching. Distances between the ATL08 data and DEM surface points (b) before and (d) after matching. Please note the vertical scale differences.

In Fig. 13, the signed distance deviations before and after DEM correction are visualised in such a way that they clearly show the scatter. It can be seen that most of the points moved from approximately -14 m before correction to close to 0 m after correction. Table VI provides an overview of the discrepancies between ICESat-2 points and DEM surface points, summarizing both the RMSE and maximum deviations.

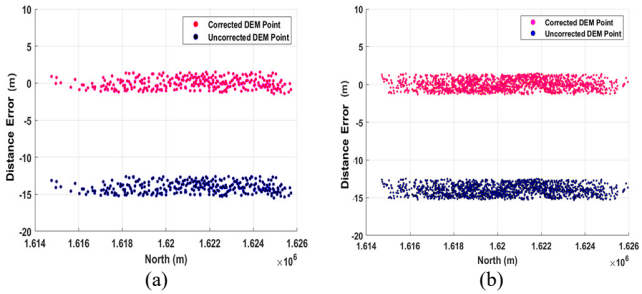


(a) (b)

Fig. 13. Signed distance errors between the ATL data and the DEM surface points, (a) for ATL08 data, (b) for ATL06 data. The blue dots refer to the distances before matching (uncorrected DEM), the red dots to the distances after matching (corrected DEM).

When using the ATL06 points, the initial RMSE was 13.9 m before the DEM correction and decreased significantly to 0.7 m after the correction. The results of the processing with the ATL08 points differ only minimally from those with the ATL06 points. Before the DEM correction, the RMSE value for ATL08 was 14.1 m, after the DEM correction it fell to 0.8 m. The maximum deviations after the DEM correction were 1.6 m for both ATL06 and ATL08 data (Table VI). This indicates that similar, high-quality DEM corrections were achievable with both datasets, and the discrepancy in the number of points (1611 ATL06 data and 320 ATL08 data) did not notably impact the results.

TABLE VI. DISTANCE ERRORS BETWEEN THE ICESAT-2 POINTS AND SURFACE POINTS OF DEM.

| Data | ATL06 points | | ATL08 points | |
|---|---|---|---|---|
| Matching | Before | After | Before | After |
| RMSE (m) | 13.9 | 0.7 | 14.1 | 0.8 |
| Max (m) | 15.2 | 1.6 | 15.4 | 1.6 |

An area within the test DEM was excluded due to image matching problems, leading to a reduced DEM accuracy in that specific area. Throughout the process of DEM bias compensation, such areas can be excluded without negatively affecting the accuracy of the correction.

A comparative analysis of the results from both test sites (Tables III and VI) reveals that the RMSE values derived from ATL08 segments of category ground at the land test site are nearly identical to the RMSE values obtained using ATL06 and ATL08 data at the Antarctic test site. Given the significant differences between terrestrial and glacial sites, and the method's comparable success when applied to both surface types, this underscores the versatility of the approach.

## V. CONCLUSION

The primary focus of this study is to investigate the feasibility of using ICESat-2 data as a substitute for conventional GCPs to correct for biases in DEMs. These biases stem from the generation of DEMs using high-resolution satellite stereo pairs together with vendor-provided RPCs. To establish an automated data flow, we have devised an algorithm for point-to-surface matching that aims at minimizing the sum

of squared distances between the points and tangential planes at the corresponding points of the DEM [23]. The ICESat-2 ATL06 and ATL08 products were tested as suitable GCPs

The experimental investigations were conducted in two distinct terrains: an easily accessible test site in Korea and a remote test site in the vicinity of the Thwaites glacier in Antarctica. The DEMs for these sites were generated using stereo images captured by KOMPSAT-3 for the Korea land test site and KOMPSAT-3A for the Antarctic test site. For the correction of the DEM with ATL08 data and the accuracy check with the ICPs, the ATL08 data was divided into the categories ground, forest, urban and all points. This categorization was accomplished through a land cover classification of the KOMPSAT multispectral image.

As anticipated, the ATL08 segments in the category ground yielded the highest accuracy in bias compensation. The deviations (RMSE) from the DEM, determined with the ICP check points, were 9.7 m prior to compensation and improved significantly to 1.2 m for the corrected DEM. With the ATL08 points of the category urban, the RMSE value rose to 2.0 m and for the category forest further up to 3.9 m. Considering segments from all three categories collectively resulted in an overall RMSE of 2.2 m.

The inclusion of terrain slope in the analysis clearly shows a strong correlation of slope and accuracy. The RMSE value of 1.2 m is confirmed for segments in the category ground for the slope range of 0-10°. Beyond a 30° slope, the RMSE increases by a factor of 7 compared to the 0-10° range.

In the Antarctic test site, the DEM correction was performed once with ATL06 data and a second time with ATL08 data. As ICPs were not available for this test site, the deviation of the ATL08 data from the corrected DEM was used as measure of the accuracy. The RMSE differed very little between ATL06 and ATL08. It was also insignificant that the ATL06 data included a much larger number of points than the ATL08 data.

Overall, the experimental outcomes underscore the potential of correcting DEMs with ICESat-2 data. The developed method has proven to be effective for the correction of DEMs created in inaccessible areas such as polar or volcanic regions, where conducting traditional GCP surveys using GNSS or other surveying techniques poses significant challenges.

## REFERENCES


[1] G. Dial, and J. Grodecki, "RPC replacement camera models," In *Proc. ASPRS Annual Conference*, Baltimore, Maryland, USA, Mar. 7-11, 2005.

[2] C.S. Fraser, and H.B. Hanley, "Bias-compensated RPCs for sensor orientation of high-resolution satellite imagery," *Photogramm. Eng. Remote Sens*., vol. 7, no. 8, pp. 909–915, Aug. 2005.

[3] X. Shen, B. Liu, and Q.-Q. Li, "Correcting bias in the rational polynomial coefficients of satellite imagery using thin-plate smoothing splines," *ISPRS J. Photogramm. Remote Sens*., vol. 125, pp. 125–131, Mar. 2017.

[4] H. Ebner, T. Ohlhof, and E. Putz, "Orientation of MOMS-02/D2 and MOMS-2P imagery," In: *Int. Arch. Photogramm. Remote Sens. Spatial Inf. Sci.,* Vienna, Vol. XXXI, Pt. B3, Com. III, pp. 158-164, July 1996.

[5] V. Helm, A. Humbert, and H. Miller, "Elevation and elevation change of Greenland and Antarctica derived from CryoSat-2," *The Cryosphere*, vol. 8, no. 4, pp. 1539–1559, Aug. 2014, doi:10.5194/tc-8-1539-2014.

[6] D. Rosenholm, and K. Torlegård, "Three-dimensional absolute orientation of stereo models using digital elevation models", *Photogramm. Eng. Remote Sens*. vol. 54, no. 10, pp. 1385–1389, Oct. 1988.

[7] H. Ebner, and G. Strunz, "Combined point determination using digital terrain models as control information," In: *Int. Arch. Photogramm. Remote Sens. Spatial Inf. Sci.*, Kyoto, Japan, Jul. 1-10, 1988.

[8] T. Kim, and J. Jeong, "DEM matching for bias compensation of rigorous pushbroom sensor models," *ISPRS J. Photogramm. Remote Sens*. vol. 66, no. 5, pp. 692–699, Sep. 2011.

[9] X. Chen, B. Zhang, M. Cen, H. Guo, T. Zhang and C. Zhao, "SRTM DEM-aided mapping satellite-1 image geopositioning without ground control points. *IEEE Geosci. Remote Sens. Lett.* Vol. 14, no. 11, pp. 2137–2141, Nov. 2017.

[10] H. Cao, P. Tao, H. Li, and J. Shi, "Bundle adjustment of satellite images based on an equivalent geometric sensor model with digital elevation model," *ISPRS J. Photogramm. Remote Sens*., vol. 156, pp. 169-183, Aug. 2019.

[11] T. Schenk, A. Krupnik, and Y. Postolov, "Comparative study of surface matching algorithms," In: *Int. Arch. Photogramm. Remote Sens. Spatial Inf. Sci.,* Amsterdam, The Netherlands, Jul. 16-23, 2000.

[12] G. Karras, and E. Petsa, "DEM matching and detection of deformation in close-range photogrammetry without control," *Photogramm. Eng. Remote Sens*., vol. 59, no. 9, pp. 1419–1424, Sep. 1993.

[13] L. Magruder, A. Neuenschwander, and B. Klotz, "Digital terrain model elevation corrections using space-based imagery and ICESat-2 laser altimetry" *Remote Sens. Environ*, vol. 264, pp. 112621-112629, Oct. 2021.

[14] X. Zhang, S. Xing, Q. Xu, G. Zhang, P. Li, and K.Chen, "Satellite remote sensing image stereoscopic positioning accuracy promotion based on joint block adjustment with ICESat-2 laser altimetry data" *IEEE Access*, vol. 9, pp. 113362-113376, Aug. 2021.

[15] J. Ye, Y. Qiang, R. Zhang, X. Liu, Y. Deng, and J. Zhang, "High-precision digital surface model extraction from satellite stereo images fused with ICESat-2 data" *Remote Sens*., vol. 14, no. 1, p. 142, Dec. 2021, doi: 10.3390/rs14010142.

[16] C. Wang, X. Zhu, S. Nie, X. Xi, D. Li, W. Zheng, and S. Chen., "Ground elevation accuracy verification of ICESat-2 data: a case study in Alaska, USA," *Opt. Exp*., vol. 27, no. 26, pp. 38168–38179, Dec. 2019.

[17] X. Tian, and J. Shan, "Comprehensive evaluation of the ICESat-2 ATL08 terrain product," *IEEE Trans. Geosci. Remote Sens*., vol. 59, no 10, pp. 8195 – 8209, Jan. 2021, doi: 10.1109/TGRS.2021.3051086.

[18] NASA Nat. Snow and Ice Data Center. *ICESat-2 science.* [Online]. Available: https://icesat-2.gsfc.nasa.gov/science, Accessed on: Sep. 2, 2020.

[19] NASA Nat. Snow and Ice Data Center. *ICESat-2 technical specs.* [Online]. Available: https://icesat-2.gsfc.nasa.gov/science/specs, Accessed on: Sep. 2, 2020.

[20] NSIDC, "ICESat-2 product overviews," NASA Nat. Snow and Ice Data Center, Boulder, CO, USA [Online]. Available: https://nsidc.org/data /icesat-2/products, Accessed on: Sep. 2, 2020.

[21] K. M. Brunt, T. A. Neumann, and B. E. Smith, "Assessment of ICESat - 2 ice sheet surface heights, based on comparisons over the interior of the Antarctic ice sheet," *Geophys. Res. Lett*., vol. 46, no. 22, pp. 13072-13078, Nov. 2019. doi: 10.1029/2019GL084886.

[22] A. L. Neuenschwander, and L. A. Magruder, "Canopy and terrain height retrievals with ICESat-2: a first look," *Remote Sens*., vol. 11, no. 14, p. 1721, Jul. 2019, doi: 10.3390/rs11141721.

[23] H. Lee, and M. Hahn, "KOMPSAT-3 digital elevation model correction based on point-to-surface matching," *Remote Sens*., vol. 11, no. 20, p. 2340, Oct. 2019, doi: 10.3390/rs11202340.

[24] H. Lee, and M. Hahn, "Point-to-surface matching for DEM correction using ICESat data," In: *Int. Arch. Photogramm. Remote Sens. Spatial Inf. Sci.,* Nice, France, Aug. 31-Sep. 02, 2020.

[25] C. C. Carabajal, and D. J. Harding, "ICESat validation of SRTM C-band digital elevation models," *Geophys. Res. Lett*., vol. 32, no. 22, pp. 1-5, Nov. 2005, doi: 10.1029/2005GL023957.

[26] K. J. Bhang, F. W. Schwartz, and A. Braun, "Verification of the vertical error in C-band SRTM DEM using ICESat and Landsat-7, Otter Tail County, MN," *IEEE Trans. Geosci. Remote Sens*., vol. 45, no. 1, pp. 36-44, Jan. 2007.